Interface effects in tunneling models with identical real and complex dispersions

Timothy B. Boykin
Department of Electrical and Computer Engineering and LICOS, The University of Alabama in Huntsville, Huntsville, Alabama 35899

Roger K. Lake
Raytheon Systems, P.O. Box 660246, MS 35, Dallas, Texas 75266

Gerhard Klimeck
Jet Propulsion Laboratory, 4800 Oak Grove Drive, MS 168-522, Pasadena, California 91109
and Raytheon Systems, P.O. Box 660246, MS 35, Dallas, Texas 75266

Mukund Swaminathan
Raytheon Systems, P.O. Box 660246, MS 35, Dallas, Texas 75266
(Received 2 March 1998; revised manuscript received 7 October 1998)

Simple heterostructure models are often employed due to their computational efficiency. The approximations involved are not, however, well understood; this is particularly true with respect to the interfaces. In order to clarify this situation we study two different monoatomic (single-band) models and two different diatomic (two-band) models all having identical dispersion relations. We study in detail the relationships between the one- and two-band models, showing that their points of agreement and disagreement arise directly from the handling of the interfaces. [S0163-1829(99)01111-X]

A recent study comparing three different bandstructure models, one- and two-band, and ten-band sp^3s^*,[1] for calculating the current-voltage characteristics of In-based resonant tunneling diodes has found that the ten-band sp^3s^* model with numerical integration over the transverse momentum and full charge self-consistency is required to make quantitative comparison with experimental results.[2] Because the electron transport in these devices takes place within the Γ valley of the conduction band, a single-band model with energy-dependent parameters mimicking the nonparabolicity of the ten-band model has been proposed as a much less computationally intensive surrogate for the more complete calculation.[3] The implementation of this parametrized single-band model[4] is very efficient and an example calculation is shown in Fig. 1.

While the one-band model with energy-dependent parameters[3,4] is clearly successful, the underlying theory remains *ad hoc*, especially the treatment of the interfaces, providing but a tenuous connection between the equations of motion of the parametrized one-band model and those of the more complete calculation it mimics. The complexity of the sp^3s^* model[1] prohibits a direct link to the parametrized one-band model; however, the one-band model may be exactly derived from a two-band calculation,[5,6] which provides the connection to the sp^3s^* model.[1] The two-band model is well suited for the study of the role played by the interfaces, and with only one orbital (s- or p_z-like) per atom effectively reproduces the Γ-valley dispersion of most III-V semiconductors along [001]. In this paper we formalize the theory by deriving from the two-band models equivalent parametrized one-band models, which exactly reproduce the physics of the conduction band for both bulk and heterointerface systems. We then discuss how these results apply to the parametrization of the ten-band sp^3s^* model.

We begin by specifying the models under study here. The two-band models are diatomic, having a single s- or p_z-like orbital per atom, the two possible configurations being s cation and p_z anion (*pa*,*sc*) or s anion and p_z cation (*sa*,*pc*). In both cases we place the anions on the Bravais lattice sites and take the orbitals to be orthonormal. These models are related via the transformations:

$$\{\varepsilon_p \rightarrow \varepsilon_s;\ \varepsilon_s \rightarrow \varepsilon_p;\ U \rightarrow -U\}, \tag{1}$$

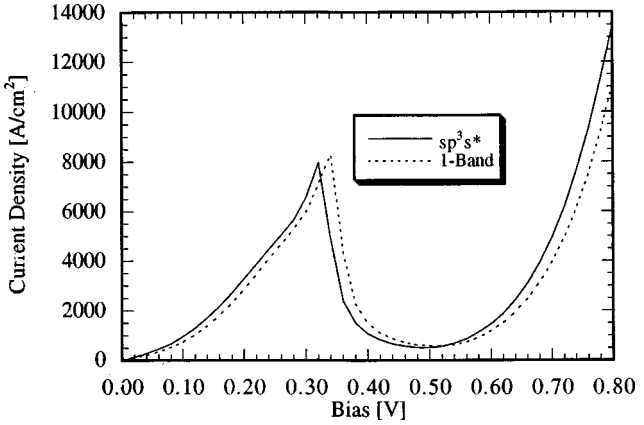

FIG. 1. Current-voltage characteristics for a double-barrier device as calculated with ten-band sp^3s^* model, labeled sp^3s^* and a one-band model, labeled one-Band; bulk regions and the 16-ML well are $In_{0.53}Ga_{0.47}As$ and each 18-ML barrier is $In_{0.52}Al_{0.48}As$. Each barrier has a 7-ML undoped spacer, the bulk regions are doped N-type $10^{18}\,cm^{-3}$ and the temperature is 300 K. These calculations include space-charge regions, but for reasons of computational convenience ignore both Hartree self-consistency (Ref. 2) and the effect of in-plane wave vector on the transmission, which accounts for the overly pronounced transmission peak (Refs. 2 and 9).

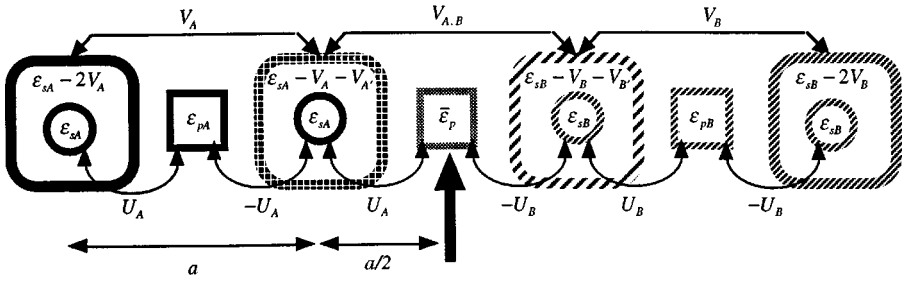

FIG. 2. The (*pa,sc*) two-band model and its one-band equivalent at an interface (indicated by the heavy arrow) between materials *A* and *B* (see text). In the two-band model cations are represented by small circles and anions by small squares. The anions occupy the Bravais lattice sites and *a* represents one-half the zinc-blende conventional unit-cell cube edge. The lattice sites for the one-band equivalent lie on the *s*-orbital positions and the one-band orbitals are represented by the large rounded squares. Two-band couplings are shown below, one-band couplings above, and onsite parameters are placed within their respective cells.

where the ε are onsite parameters and we take the couplings U to be real. The (*pa,sc*) version is the more often employed since its conduction-band wave function near Γ is mostly *s*-cation, like that of the sp^3s^* model.[1] We treat common anion materials systems, so that at a heterointerface we average the onsite anion matrix element and take the left- and right-coupling parameters to be their respective bulk values.

The one-band model has an *s*-like orbital on each lattice site; again, the orbitals are orthonormal. Although the equations of the one-band model are formally equivalent to those of the discretized effective-mass Schrödinger equation, we adopt the tight-binding viewpoint for it. This picture suggests interface conditions different from those typically chosen in discretized effective-mass models.[7]

Both the bulk and heterostructure electronic properties are found by solving the Schrödinger equation in the planar-orbital basis. For the one-band model we write the wave function as a superposition of localized *s*-like orbitals centered on each site,

$$|\Psi\rangle=\sum_{n'} C_{n'}|n'a\rangle, \tag{2}$$

while for the two-band model we have

$$|\Psi\rangle=\sum_{n'} \{C^{\mu}_{n'}|\mu;n'a\rangle+C^{\nu}_{n'}|\nu;n'a+a/2\rangle\}, \tag{3}$$

where $(\mu,\nu)=(p,s)$ for the (*pa,sc*) version and $(\mu,\nu)=(s,p)$ for the (*sa,pc*). In both Eqs. (2) and (3) *a* represents one-half of the zinc blende conventional unit-cell cube edge. Taking inner products of the localized orbitals with the Schrödinger equation yields equations for the expansion coefficients, *C*. Since the interface equations are the more general, we consider them first.

In the two-band models we consider a heterointerface at cell 0 between materials *A* and *B* (i.e., $A\rightarrow B$) in order to establish the relationship between them and the one-band model (Figs. 2, 3). For the (*pa,sc*) two-band model we need both the equation at the interface itself and the pair of bulk-like equations on each side. Those for material *A* leading up to and including the interface are

$$U_AC^s_{-2}+[\varepsilon_{pA}-E]C^p_{-1}-U_AC^s_{-1}=0, \tag{4}$$

$$-U_AC^p_{-1}+[\varepsilon_{sA}-E]C^s_{-1}+U_AC^p_0=0, \tag{5}$$

$$U_AC^s_{-1}+[\bar{\varepsilon}_p-E]C^p_0-U_BC^s_0=0. \tag{6}$$

Note that two bulk *B* equations, of the forms (5) and (4), follow Eq. (6). For the (*sa,pc*) two-band model, we need only the equations at and straddling the interface:

$$U_AC^s_{-1}+[\varepsilon_{pA}-E]C^p_{-1}-U_AC^s_0=0, \tag{7}$$

$$-U_AC^p_{-1}+[\bar{\varepsilon}_s-E]C^s_0+U_BC^p_0=0, \tag{8}$$

$$U_BC^s_0+[\varepsilon_{pB}-E]C^p_0-U_BC^s_1=0. \tag{9}$$

From these equations we find the equivalent one-band models with energy-dependent parameters by eliminating the C^p_j from Eqs. (4)–(6) or Eqs. (7) and (8) and replacing $C^s_j\rightarrow C_j$. For the (*pa,sc*) two-band model this results in a one-band equivalent in which the interface lies between the cells (Fig. 2), characterized by two equations:

$$-\frac{U_A^2}{E-\varepsilon_{pA}}C_{-2}+\left[\varepsilon_{sA}-E+\frac{U_A^2}{E-\varepsilon_{pA}}+\frac{U_A^2}{E-\bar{\varepsilon}_p}\right]C_{-1}-\frac{U_AU_B}{E-\bar{\varepsilon}_p}C_0=0, \tag{10}$$

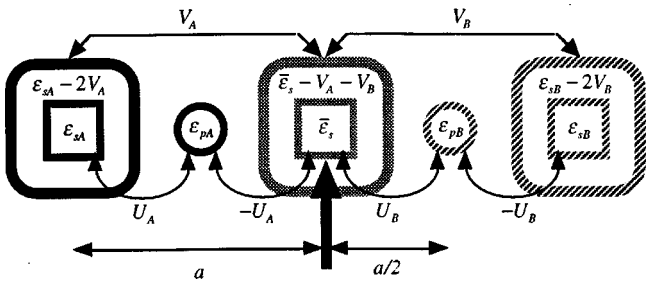

FIG. 3. The (*sa,pc*) two-band model and its one-band equivalent at an interface (indicated by the heavy arrow) between materials *A* and *B* (see text). In the two-band model cations are represented by small circles and anions by small squares. The anions occupy the Bravais lattice sites and *a* represents one-half the zinc blende conventional unit-cell cube edge. The lattice sites for the one-band equivalent lie on the *s*-orbital positions and the one-band orbitals are represented by the large rounded squares. Two-band couplings are shown below, one-band couplings above and onsite parameters are placed within their respective cells.

$$-\frac{U_A U_B}{E-\overline{\varepsilon_p}}C_{-1}+\left[\varepsilon_{sB}-E+\frac{U_B^2}{E-\overline{\varepsilon_p}}+\frac{U_B^2}{E-\varepsilon_{pB}}\right]C_0 - \frac{U_B^2}{E-\varepsilon_{pB}}C_1=0. \tag{11}$$

Equation (10) results from applying the elimination procedure to Eqs. (4)–(6) while Eq. (11) results from its application to Eq. (6) and the two bulk B equations that follow. The one-band equivalent to the (*sa*,*pc*) two-band model arises from Eqs. (7)–(9). Its interface occurs at a cell (Fig. 3) and is characterized by the single equation

$$-\frac{U_A^2}{E-\varepsilon_{pA}}C_{-1}+\left[\overline{\varepsilon_s}-E+\frac{U_A^2}{E-\varepsilon_{pA}}+\frac{U_B^2}{E-\varepsilon_{pB}}\right]C_0 - \frac{U_B^2}{E-\varepsilon_{pB}}C_1=0. \tag{12}$$

These derivations ensure that each one-band model exactly mimics the conduction band of its respective two-band antecedent over the entire bandwidth, the difference in wave functions (purely *s*-like versus an energy-dependent mixture of *s*- and *p*-like components) notwithstanding.

The above interface equations are more easily interpreted in view of the bulk relationships, found by setting $A=B$ and imposing Bloch's theorem on the coefficients C. In bulk we require the conduction band of both versions of the two-band model to be purely *s*-like at $k=0$. For either version of the two-band model, then, we find for the conduction (+) and (light-hole) valence (−) band dispersion relations

$$E_{\pm}^{(2)}(k)=\frac{\varepsilon_s+\varepsilon_p}{2}\pm\sqrt{\left(\frac{\varepsilon_s-\varepsilon_p}{2}\right)^2+4U^2\sin^2\left(\frac{ka}{2}\right)}. \tag{13}$$

Note that Eq. (13) gives $m_{lh}=-m_e$ and determines ε_s, ε_p, and U in terms of the band edges and effective mass at $k=0$: $E_+(0)=\varepsilon_s$, $E_-(0)=\varepsilon_p$, $E_g(0)=\varepsilon_s-\varepsilon_p$, and $U^2=\hbar^2E_g(0)/(2a^2m_e)$. For the one-band model, the (conduction-band) dispersion is given by

$$E^{(1)}(k)=\varepsilon+2V\cos(ka). \tag{14}$$

The energy-dependent parameters of the one-band model are directly read off of the bulk versions of Eqs. (10), (11), or (12). The coupling parameters are (for $E>\varepsilon_p$)

$$V=-\frac{U^2}{E-\varepsilon_p}, \tag{15}$$

while the onsite parameters retain their usual form,

$$\varepsilon=\varepsilon_s-2V. \tag{16}$$

Note that at the conduction-band edge V becomes the usual one-band coupling parameter $V=-\hbar^2/(2a^2m_e)$ and that since these were derived from the equations of motion in the planar-orbital basis they apply for both propagating and evanescent states. Using bulk dispersion relations (13) and (14) we may write the energy-dependent coupling V as

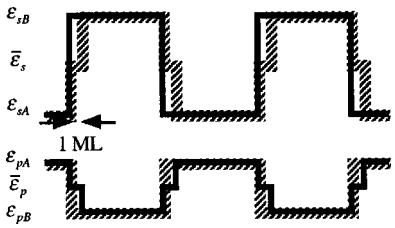

FIG. 4. Approximate band-edge diagrams for the two-band models showing the effects of averaging the interfacial anion parameter. Solid: (*pa*,*sc*), same-site *p*-parameter averaged ($\overline{\varepsilon_p}$); shaded: (*sa*,*pc*), same-site *s*-parameter averaged ($\overline{\varepsilon_s}$).

$$V=\frac{E_+^{(2)}(k)-\varepsilon_s}{2[\cos(ka)-1]}. \tag{17}$$

With $E^{(2)}{}_+(k)$ replaced by the ten-band dispersion and ε_s by the conduction-band minimum, Eqs. (16) and (17) are the energy-dependent parameters used in the one-band calculation of Fig. 1; this parametrization differs from that described in Ref. 3.

These bulk relations explain the onsite and coupling parameters appearing in the equivalent one-band interface Eqs. (10)–(12). The single-band equivalent to the (*sa*,*pc*) model has an interface occurring at a lattice site and its onsite parameter is the average of the bulk A and B values while the left and right couplings are those for bulk A and B, respectively. Conversely, the (*pa*,*sc*) model produces a one-band model with an interface between the lattice sites, as is conventional in discretized effective-mass models. While Eqs. (10) and (11) have clear interpretations in terms of *s*-state energies being altered by their couplings to *p* states, the interface coupling parameters do not follow any normal single-band rule.[7] Indeed, the interfacial coupling parameter,

$$V_{A,B}=-\frac{U_A U_B}{E-\overline{\varepsilon_p}} \tag{18}$$

is not an arithmetic or, except in the special case of zero valence-band offset, a geometric mean of the bulk parameters V_A and V_B. Furthermore, $V_{A,B}$ appears in neither of the onsite terms adjacent to the interface, $-U_A{}^2/(E-\overline{\varepsilon_p})$ and $-U_B{}^2/(E-\overline{\varepsilon_p})$, taking its place on the left and right, respectively. Although $V_{A,B}$ is the geometric mean of these nonbulk terms, we show below that it has a more physical interpretation. Finally, the valence-band edge in these nonbulk terms is $\overline{\varepsilon_p}$.

These differences among the models manifest themselves in terms of the conduction- and valence-band profiles. For heterointerfaces between materials having similar gap-to-mass ratios (most III-V semiconductors) the two-band coupling parameters U on either side will be similar, so that the interfacial monolayer is essentially one-unit-cell of a bulk crystal with band edges given by its *s*- and *p*-onsite parameters. In the (*sa*,*pc*) two-band model at an $A\rightarrow B$ interface (left-most interface in Fig. 4, shaded) the approximate conduction- and valence-band edges are $\overline{\varepsilon_s}$ and ε_{pB}, respectively, the averaged interfacial onsite parameter producing a step in the conduction band, likewise reflected through $\overline{\varepsilon_s}$ in the onsite-interface one-band model. In contrast, the (*pa*,*sc*) two-band model has approximate interfacial edges ε_{sB} and

$\overline{\varepsilon_p}$ (Fig. 4, solid) producing a valence-band step, as noted above for the inbetween-site interface one-band model. The nonbulk parameters in Eqs. (10)–(12) clearly reflect the alloy nature of the interfaces, a point missed in effective-mass descriptions. In Eq. (12) the alloying is obvious. In Eq. (10) and (11) it shows in both the onsite and interfacial coupling parameters. The onsite parameters of cells -1 and 0 appear as materials A', with band edges ε_{sA} and $\overline{\varepsilon_p}$ and coupling U_A, and B', with band edges ε_{sB} and $\overline{\varepsilon_p}$ and coupling U_B, respectively. The interfacial coupling (18) is also that of an alloy, since $V_{A,B}=2V_{A'B'}-(V_{A'}+V_{B'})/2$, where the V_a are energy-dependent parameters, [Eq. (15)], for materials A', B', and $A'B'$, the last defined by two-band parameters $\overline{\varepsilon_s}$, $\overline{\varepsilon_p}$, and $\overline{U}=(U_A+U_B)/2$. Physically, $V_{A'B'}$ belongs to the one-band equivalent of the two-band alloy $A'B'$, while $(V_{A'}+V_{B'})/2$ is the coupling parameter produced by alloying one-band equivalents of A' and B'.

The foregoing analysis is also valuable for determining the applicability of simpler (parametrized one-band or two-band) models as surrogates for more complete calculations, e.g., sp^3s^*.[1] The expressions for the conduction- and valence-band extrema at Γ in the nearest-neighbor sp^3s^* model[8] show that the usual common-anion boundary condition, averaging the on-site interfacial anion parameters, produces steps in both the conduction and valence bands. (These steps generally are not the simple arithmetic averages of the two-band models.) Since the bulk wave functions even at $\mathbf{k}=0$ contain both anion and cation components, the extent to which the steps affect the electronic properties of a given heterostructure is therefore materials- and structure-dependent. It is nevertheless clear that the nearest-neighbor sp^3s^* (Ref. 1) interfaces represent an intermediate between the limiting cases of the (*pa*,*sc*) and (*sa*,*pc*) models, generally weighted more toward the (*pa*,*sc*). It is also apparent from the differences between the parametrized one-band equations and those of the conventional discretized effective-mass model that a one-band model requires only Hermiticity, not strict adherence to the usual effective-mass equations, and that the interface coupling parameter ought to represent some kind of alloy.

Indeed, our analysis suggests how to determine the onsite and coupling elements of a parametrized single-band model for an sp^3s^* calculation. If an onsite interface is desired, Eq. (12) shows that the onsite parameter must be $(\varepsilon_{c,A}+\varepsilon_{c,B})/2-V_A-V_B$, where the ε_c are the conduction-band edges and the V are given by Eq. (17) with the relevant bulk dispersion and conduction-band edge replacing $E^{(2)}{}_+(k)$ and ε_s, respectively. For the usual inbetween site interface, the onsite terms in Eqs. (10) and (11) should be $\varepsilon_{c,A}-V_A-V_{A'}$ and $\varepsilon_{c,B}-V_B-V_{B'}$, respectively, where $V_{M'}(M=A,B)$ are alloy parameters of the form (17). While there are several reasonable ways to generate the sp^3s^* parameters for alloy M', one is to replace the onsite anion parameters in the bulk-*M* set with the averages of their bulk-*A* and bulk-*B* values. The interfacial coupling $V_{A,B}$ could be either the geometric mean of $V_{A'}$ and $V_{B'}$, or $V_{A,B}=2V_{A'B'}-(V_{A'}+V_{B'})/2$ as above, where the sp^3s^* parameters for material $A'B'$ are given by the averages of those for *A* and *B*.

We have studied the equations of motion for two different two-band models, deriving for each an equivalent one-band model with energy-dependent parameters, valid for both bulk and interface systems. We find that the (*sa*,*pc*) two-band model produces a one-band model with onsite interfaces while the (*pa*,*sc*) two-band model produces a single-band model with interfaces between sites and that in neither case do these interface equations agree with those of the conventional discretized effective-mass model. We have seen that the two-band common-anion interface approximately results in a step in the conduction band for the (*sa*,*pc*) two-band model, but gives a valence-band step in the (*pa*,*sc*) two-band model and that these steps likewise occur in the respective one-band models. We have furthermore noted that the interfaces in the sp^3s^* model[1] represent intermediates between the extremes of those in the simple models so that their suitability as surrogates for sp^3s^* calculations will be materials and structure dependent, generally better for thicker layers. Our analysis shows the importance of incorporating the alloy nature of the heterointerfaces into a parametrized one-band model, and that this critical alloy behavior is largely missed in conventional effective-mass treatments.

T.B.B. thanks NSF-EPSCoR for support through Alabama EPSCoR Cooperative Agreement No. NSF 9720653.

[1] P. Vogl, Harold P. Hjalmarson, and John D. Dow, J. Phys. Chem. Solids **44**, 365 (1983).

[2] R. Chris Bowen, Gerhard Klimeck, Roger K. Lake, William R. Frensley, and Ted Moise, J. Appl. Phys. **81**, 3207 (1997).

[3] R. Lake, G. Klimeck, R. C. Bowen, D. Jovanovic, D. Blanks, and M. Swaminathan, Phys. Status Solidi B **204**, 354 (1997).

[4] M. Swaminathan, R. Lake, and G. Klimeck (unpublished).

[5] G. A. Sai-Halasz, L. Esaki, and W. A. Harrison, Phys. Rev. B **18**, 2812 (1978).

[6] J. N. Schulman, J. Appl. Phys. **60**, 3954 (1986).

[7] C. Juang, K. J. Kuhn, and R. B. Darling, Phys. Rev. B **41**, 12 047 (1990).

[8] Timothy B. Boykin, Gerhard Klimeck, R. Chris Bowen, and Roger Lake, Phys. Rev. B **56**, 4102 (1997).

[9] Timothy B. Boykin, R. E. Carnahan, and K. P. Martin, Phys. Rev. B **51**, 2273 (1995).